Published in final edited form as:
*J Neuroimmune Pharmacol*. 2013 March ; 8(1): 262–273. doi:10.1007/s11481-012-9416-6.

# Nanoprobing of the effect of $Cu^{2+}$ cations on misfolding, interaction and aggregation of amyloid β peptide

**Zhengjian Lv**[#], **Margaret M. Condron**[†], **David B. Teplow**[†,§], and **Yuri L. Lyubchenko**[#,*]

[#]Department of Pharmaceutical Sciences, University of Nebraska Medical Center, 986025 Nebraska Medical Center, Omaha, Nebraska 68198

[†]Department of Neurology, David Geffen School of Medicine at UCLA

[§]Molecular Biology and Brain Research Institutes, and Mary S. Easton Center for Alzheimer's Disease Research at UCLA, David Geffen School of Medicine at UCLA, Los Angeles, CA 90095

## Abstract

Misfolding and aggregation of the amyloid β-protein (Aβ) are hallmarks of Alzheimer's disease. Both processes are dependent on the environmental conditions, including the presence of divalent cations, such as $Cu^{2+}$. $Cu^{2+}$ cations regulate early stages of Aβ aggregation, but the molecular mechanism of $Cu^{2+}$ regulation is unknown. In this study we applied single molecule AFM force spectroscopy to elucidate the role of $Cu^{2+}$ cations on interpeptide interactions. By immobilizing one of two interacting Aβ42 molecules on a mica surface and tethering the counterpart molecule onto the tip, we were able to probe the interpeptide interactions in the presence and absence of $Cu^{2+}$ cations at pH 7.4, 6.8, 6.0, 5.0, and 4.0. The results show that the presence of $Cu^{2+}$ cations change the pattern of Aβ interactions for pH values between pH 7.4 and pH 5.0. Under these conditions, $Cu^{2+}$ cations induce Aβ42 peptide structural changes resulting in N–termini interactions within the dimers. $Cu^{2+}$ cations also stabilize the dimers. No effects of $Cu^{2+}$ cations on Aβ–Aβ interactions were observed at pH 4.0, suggesting that peptide protonation changes the peptide-cation interaction. The effect of $Cu^{2+}$ cations on later stages of Aβ aggregation was studied by AFM topographic images. The results demonstrate that substoichiometric $Cu^{2+}$ cations accelerate the formation of fibrils at pH 7.4 and 5.0, whereas no effect of $Cu^{2+}$ cations was observed at pH 4.0. Taken together, the combined AFM force spectroscopy and imaging analyses demonstrate that $Cu^{2+}$ cations promote both the initial and the elongation stages of Aβ aggregation, but protein protonation diminishes the effect of $Cu^{2+}$.

### Keywords

Amyloid β-protein; Aβ42; Alzheimer's disease; $Cu^{2+}$ cations; Single molecule force spectroscopy; Atomic force microscopy imaging

## Introduction

Misfolding and aggregation of the amyloid β–protein (Aβ) peptide are two of the key features of Alzheimer's disease (AD) (Dobson 2003), which has no cure at the present time.

[*]Corresponding author: Yuri L. Lyubchenko, Department of Pharmaceutical Sciences, University of Nebraska Medical Center, Omaha, NE, 68198 Phone: 402-559-1971; Fax: 402-559-9543, ylyubchenko@unmc.edu.

**Conflict of Interest**

The authors declare that they have no conflict of interest.

Supporting Information Available: The estimation of contour length of all tethers; the force spectroscopy results in the presence and absence of $Cu^{2+}$ cations at pH 6.8 and 6.0. This material is available free of charge *via* the Internet.

Aβ peptide, including residues 39–43, is capable of forming aggregates of various morphologies, including fibrils (Bitan et al. 2003; Ono et al. 2009). Several lines of evidence suggest that $Cu^{2+}$ cations play an important role in the aggregation of Aβ42 both *in vitro* and *in vivo*. For example, a prominent characteristic of AD is altered $Cu^{2+}$ concentrations in the brain and disrupted $Cu^{2+}$ homeostasis (Roberts et al. 2012). $Cu^{2+}$ ions are found concentrated within senile plaques of AD patients directly bound to Aβ with a picomolar affinity (Hong and Simon 2011). The concentration of $Cu^{2+}$ within the senile plaques of AD patients is 26 times higher than within the extracellular space of healthy individuals (Chen et al. 2011). Aβ plaques are therefore considered a metal "sink" (Atwood et al. 1998). Copper in a high-cholesterol diet induces amyloid plaque formation and learning deficits in a rabbit model of AD (Sparks and Schreurs 2003). Trace amounts of metal cations initiate and promote Aβ aggregation (Huang et al. 2004; Innocenti et al. 2010). Moreover, metal cations are believed to contribute to AD pathogenesis by causing oxidative stress, which could lead to the dysfunction or death of neuronal cells (Jomova et al. 2010; Barnham et al. 2004). One of the prevailing underlying mechanisms of AD etiology is the metal–triggering hypothesis (Hung et al. 2010; Rivera-Mancia et al. 2010).

Although a few papers report inhibitory effects of $Cu^{2+}$ cations on Aβ aggregation (Zou et al. 2001), it is generally accepted that $Cu^{2+}$ cations promote Aβ aggregation (Faller 2009; Lin et al. 2010). However, the end products of Aβ aggregation in the presence of $Cu^{2+}$ cations remain unclear. Whether $Cu^{2+}$ cations accelerate the growth of Aβ42 fibrils has been vigorously debated in recent years. The published results have been confusing and, to some extent, contradictory. Both amorphous aggregates and fibrils were reported to be end products (Miura et al. 2000; Tougu et al. 2011), indicating the complexity of the $Cu^{2+}$–Aβ interaction. It is now understood that the $Cu^{2+}$–Aβ interaction is sensitive to experimental conditions (Olubiyi and Strodel 2012; Klug et al. 2003), such as pH, Aβ concentration, ionic strength, temperature, and agitation. A minor change in experimental conditions may lead to different morphologies of Aβ aggregates. The effect of metal cations on Aβ aggregation is also metal/sequence-specific (Dong et al. 2007). Copper cations accelerated fibril formation of Aβ (14–23), but inhibited formation of Aβ (11–23) and Aβ (11–28) (Faller and Brown 2009).

Despite the fact that the effects of $Cu^{2+}$ cations on Aβ aggregation have been extensively investigated, the underlying mechanism controlling aggregation remains elusive. One of the main challenges is obtaining detailed $Cu^{2+}$–Aβ42 interaction information during the earliest stage of aggregation, especially in the dimerization phase, because oligomers are transient states not amenable to traditional visualization techniques. In addition, the ability of $Cu^{2+}$ cations to promote the growth of fibrils needs to be verified. Therefore, a thorough study capable of probing transient states of $Cu^{2+}$–Aβ42 interactions at the single molecule level would be significant.

Recently, the single molecule force spectroscopy (SMFS) mode of atomic force microscopy (AFM) has been used to detect the specific interaction forces of biological molecules (Krasnoslobodtsev et al. 2007; Sulchek et al. 2005). We recently succeeded in using SMFS to characterize the early stage of Aβ and α–synuclein aggregation (Kim et al. 2011; Yu et al. 2011). These studies revealed the high stability of Aβ and α–synuclein misfolded dimers and led to a novel hypothesis explaining the role of dimerization in amyloid protein misfolding and aggregation (Lyubchenko et al. 2010). Furthermore, by using SMFS, we examined the effects of $Zn^{2+}$ and $Al^{3+}$ on the early stages of α–synuclein aggregation at neutral pH (Yu et al. 2011). The results demonstrated that $Zn^{2+}$ and $Al^{3+}$ greatly promote the dimerization of α–synuclein. It is thus reasonable to extend the use of AFM to inspect the effect of $Cu^{2+}$ cations on Aβ42 aggregation. The application of AFM and SMFS can provide direct information about Aβ aggregation at the nanometer level.

In this paper, we report on data from our SMFS and AFM imaging studies to elucidate the effect of $Cu^{2+}$ cations on interactions of Aβ42 peptides during the initial stages of aggregation and on the growth of aggregates at later stages. The role of pH on $Cu^{2+}$–Aβ42 interactions is also discussed. We find that $Cu^{2+}$ cations change the interaction pattern of Aβ42 dimers and accelerate the aggregation process by promoting fibrillogenesis, but these effects are abolished in acidic conditions. These results may have relevance for understanding the etiology of AD and for development of knowledge-based drug design strategies targeting metal − Aβ interactions.

## Materials and methods

### Materials

Aβ42 (CDAEFRHDSGYEVHHQKLVFFAEDVGSNKGAIIGLMVGGVVIA) was synthesized using 9-fluorenylmethoxycarbonyl (Fmoc) chemistry and purified by reverse phase high performance liquid chromatography (RP-HPLC). The identity and purity (usually >97%) of the peptides were confirmed by amino acid analysis followed by mass spectrometry and reverse phase high performance liquid chromatography (RP-HPLC). The lyophilized Aβ42 was dissolved in TFA (2 mg/ml) by ultrasonication (Branson 1210) for 5 min to destroy dimeric and higher oligomers and then dried immediately using a vacuum centrifuge (Vacufuge, Eppendorf). The white powder of Aβ42 was dissolved at 2 mg/ml in dimethyl sulfoxide (DMSO) as a stock solution and then diluted in DMSO before being used. The final concentration of diluted Aβ42 was determined by spectrophotometry (Nanodrop® ND–1000). The molar extension coefficients used for tyrosine and cysteine were 1280 $cm^{-1}{\cdot}m^{-1}$ and 120 $cm^{-1}{\cdot}m^{-1}$, respectively. Stock solutions of cysteinyl-Aβ42 were prepared as previously described (Kim et al. 2011; Yu et al. 2008; Walsh et al. 1997).

A 50 mM 1–(3–aminopropyl) silatrane (APS) stock solution was prepared by dissolving the APS powder in DI water. The 1.67 mM stock solution of maleimide–polyethylene glycol–succinimidyl valerate (MAL–PEG–SVA; 3.4 kDa Laysan Bio Inc, Arab, AL) was prepared in DMSO (Sigma–Aldrich Inc.) and stored at −20°C. The 10 mM Tris (2–carboxyethyl) phosphine (TCEP) hydrochloride (Hampton Research Inc.) and the 2.94 mM stock solution of maleimide silatrane (MAS) were prepared in DI water and stored at −20°C. A 20 mM stock solution of β–mercaptoethanol was prepared in pH 7.4 buffer and kept under room temperature.

Copper chloride ($CuCl_2$) was purchased from Sigma–Aldrich and used without additional purification. A 1 mM stock solution of $CuCl_2$ was prepared by dissolving the $CuCl_2$ powder into DI water. Glycine was added into the buffer solutions at pH 7.4 and 6.0 to stabilize the $CuCl_2$ stock solution. The $CuCl_2$ solutions with different pH values were all diluted to a final concentration of approximately 1–5 μM. Other reagents used in the experiments were of analytical grade from Sigma–Aldrich, unless otherwise specified. Deionized water (18.2 MΩ, 0.22 μm pore size filter, APS Water Services Corp., Van Nuys, CA) was used for all experiments.

### Buffer solutions

Buffers were 50 mM 4–(2–hydroxyethyl)–1–piperazineethanesulfonic acid (HEPES) (pH 7.4), 20 mM 3–(N–morpholino) propanesulfonic acid (MOPS) (pH 6.8), 20 mM monopotassium phosphate (pH 6.0), and 10 mM sodium acetate (pH 5.0 and 4.0). All buffer solutions were adjusted to a final ionic strength of 150 mM using sodium chloride and were filtered through 0.22 μm disposable nylon filters before use.

### Functionalization of AFM tips

The functionalization of AFM tips and mica surfaces were done as described previously (Yu et al. 2008; Yu and Lyubchenko 2009). Briefly, silicon nitride ($Si_3N_4$) AFM tips (MSNL–10, Veeco) were immersed in 100% ethanol solution for 15 min, rinsed thoroughly with water, dried with argon, and then exposed to UV light (CL–1000 Ultraviolet Crosslinker, UVP, Upland, CA) for 30 min. The AFM tips were placed in an aqueous solution of 167 μM MAS for 3 h followed by multiple thorough rinses with water. A 20 nM Aβ42 peptide solution in pH 7.4 HEPES buffer solution was pretreated with 20 μM TCEP hydrochloride for 15 min to break any intermolecular disulfide bonds between the Aβ42 molecules and ensure that the covalently attached Aβ42 molecules were in monomeric form. The MAS–modified AFM tips were immersed into the above mentioned peptide solution for 1 h to covalently attach the peptides. After rinsing with pH 7.4 HEPES buffer, the Aβ42 peptide–tethered AFM tips were treated with 10 mM β–mercaptoethanol solution for 10 min to block the unreacted maleimide moieties. Finally, the Aβ42 peptide–functionalized AFM tips were washed with pH 7.4 HEPES and stored in the same buffer. Typically, the storage time was less than 24 h.

### Modification of mica surfaces

Mica sheets (Asheville–Schoonmaker Mica Co., Newport News, VA) were cut into 1.5 cm × 1.5 cm squares. The freshly cleaved mica surfaces were treated with APS for 30 min followed by reaction with 167 μM MAL–PEG–SVA in DMSO. After activation for 3 h, the mica squares were rinsed sequentially with DMSO and water to remove unbound MAL–PEG–SVA, and then dried with argon. The remaining steps for immobilizing the Aβ42 peptides onto the mica surface were the same as described above for the AFM tips.

### Single molecule force spectroscopy

The single molecule force spectroscopy force measurements were conducted in different pH buffer solutions at room temperature with the Molecular Force Probe 3D AFM system (MFP 3D, Asylum Research, Santa Barbara, CA). AFM probes with nominal spring constants of 0.03 N/m were used throughout the experiments. The apparent spring constants were calibrated by the thermal noise analysis method with the Igor Pro 6.04 software (provided by the manufacturer). A low trigger force (100 pN) was exerted on the AFM probes. The retraction velocity of all experiments was set at 500 nm/s. At each pH, force measurements between Aβ42–functionalized AFM tips and Aβ42–modified mica were first performed in the absence of $Cu^{2+}$ and then in the presence of $Cu^{2+}$. The tip and mica remained intact in the presence of $Cu^{2+}$. For each force measurement, at least 100 rupture events were collected over at least three randomly chosen locations on the mica surface to allow accurate statistical analysis. Force curves were obtained by probing over area 5×5 μm generating force maps each sized in 60 × 40 points. It took 35~75 min to finish a single force map; the time depends on the retraction velocity. The sampling rate for each force curve varied from 1 kHz to 2 kHz. By using the exact same experimental setup, the same concentration of Aβ42, and the same type of AFM tips throughout all experiments, several attempts of force probing were made for each experiment. Therefore, it was reasonable to calculate the yield of rupture events by averaging the numbers of yield obtained from a set of repeating experiments.

### Tapping mode AFM imaging

The growth of Aβ fibrils in the absence and presence of $Cu^{2+}$ was monitored with tapping mode AFM (Nanoscope V, Veeco). Aβ stock solutions were diluted with a working buffer solution and filtered through a 10 kDa filter unit (Amicon® Ultra) by centrifuging at 16,873 × *g* for 15 min. The final Aβ concentration was 10 μM for all imaging experiments.

Substoichiometric $Cu^{2+}$ cations were added in Aβ solutions at a molar ratio of 1:10. $Cu^{2+}$ free Aβ solutions also were prepared in parallel as control experiments. All Aβ solutions were incubated at 37°C under quiescent conditions. Samples for AFM imaging were prepared every day to check the progress of aggregation. After each sample preparation, 4 μL of the incubated solution was deposited on a freshly cleaved bare mica surface, which was immobilized on a metal disc via a double–sided sticker. The solution was allowed to sit for 2 min to let the Aβ aggregates absorb onto the mica surface. The mica surface was rinsed with DI water to remove any soluble solvents. The mica surface was then dried with argon and placed into a vacuum chamber for at least 3 h, after which imaging was performed. Images with typical features (5×5 μm in size) were acquired at a scan rate of 1 Hz and resolution of 512×512.

## Data analysis

Three rules were applied to select force–distance curves: 1) according to the thermal noise of the experimental setup, the rupture forces should be higher than 20 pN; 2) the contour lengths (the length at maximum physically possible extension of the interaction system determined after the WLC analysis) should be larger than 20 nm (see Results below); 3) the distance of the tip-sample separation (the projection of distance between AFM tip and mica substrate on the vertical axis) should be larger than 15 nm to exclude the nonspecific interactions between the tip and bare mica. All force curves which did not meet the above requirements were discarded. Overlapping of raw rupture forces was accomplished by using Igor Pro software.

The worm like chain (WLC) model was used for fitting the force-distance curves:

$$F(x)=\frac{k_B T}{L_p}\left[\frac{1}{4}\left(1-\frac{x}{L_c}\right)^{-2}-\frac{1}{4}+\frac{x}{L_c}\right] \quad (1)$$

where $F(x)$ is the force at the distance of $x$, $k_B$ is the Boltzman constant, $T$ is the absolute temperature, and $L_p$ and $L_c$ are the persistence length and the contour length, respectively. The persistence length of PEG was fixed at 0.38 nm (Gomez-Casado et al. 2011). From the WLC fit of force distance curves, the contour lengths were obtained with the Igor Pro 6.04 software package.

The apparent loading rates were calculated by using the following equation (Yu et al. 2011):

$$\frac{1}{r}=\frac{1}{k_c v}\left(1+\frac{k_c L_c}{4}\sqrt{\frac{F_p}{F^3}}\right) \quad (2)$$

where $F_p = k_B T/L_p$, $k_c$ is the spring constant (pN/nm), $v$ is the tip velocity, $F$ is the rupture force, and $r$ is the apparent loading rate (pN/s). All histograms were generated by Origin 7.0 software and fitted with a Gaussian distribution. Data are shown in the form of mean ± SD.

Quantitative analysis of Aβ aggregates was achieved by using Femtoscan Online software (Advanced Technologies Center, Moscow, Russia) (Portillo et al. 2012). The background was initially subtracted to eliminate anything that was less than 1 nm in height. The “enum features” function was used to count the particle number and read out information about shape and height. This function can be used to determine the elongation factor of the Aβ aggregates, which is represented as Rs/Rp (the ratio between two radii in an oblong object), also known as form factor. Form factors were interpreted as follows: 0–0.5 represented mature fibrils; 0.5–0.8 represented protofibrils; and 0.8–1.0 represented oligomers. The percentages of various Aβ aggregates were calculated and shown as pie charts.

# Results

## Experimental setup of SMFS

It is a widely acknowledged fact that Aβ aggregation must begin with peptide dimerization. Therefore, we rationalized that immobilization of Aβ42 monomers on the tip and the mica surface would represent a pivotal step in order to analyze the initial stages of aggregation. Our experimental setup is illustrated in Fig. 1a. One of the interacting Aβ42 molecules is anchored onto the AFM tip through a short linker, MAS, and a second Aβ42 molecule is immobilized on the mica surface using a long PEG linker. Specific interaction forces between these molecules were measured by multiple approach-retraction cycles. Treating the Aβ42 solution with TCEP efficiently reduces cystine links that create Aβ dimers (Kim et al. 2011). Therefore, the Aβ42 molecules used for immobilization were single monomers. In addition, we took advantage of the presence of the maleimide group exclusively covalently coupled to the cysteine group at the N–terminus of Aβ42. The concentration of Aβ42 peptide used in the current study was as low as 20 nM, therefore this site-specific attachment would result in sparse surface presentation of Aβ42 molecules onto the mica surface and AFM tip, preventing peptide aggregation during the immobilization step (Yu et al. 2011; Kim et al. 2011). Additionally, the concentration of Aβ42 peptide used was more than three orders of magnitude less than that used in aggregation experiments *in vitro* (Kim et al. 2011; Yu et al. 2011). Bifunctional PEG was chosen to circumvent unwanted nonspecific interactions between the AFM tip and the mica surface, and to function as a spacer to sort out the nonspecific interactions that often take place between tips and substrates with a short separation.

Fig. 1b shows a typical rupture force–distance curve with a clear peak located at a distance defined primarily by linker stretching that could be associated with the specific interactions between Aβ42 molecules. Prior to this rupture peak, a section of a parabolic curve exists that originates from stretching of the extendable segments of the linkers and the interacting molecules.

## Effect of $Cu^{2+}$ cations on the Aβ42 interaction

The effect of $Cu^{2+}$ cations on the Aβ42 interaction was investigated by SMFS at pH values of 7.4, 6.8, 6.0, 5.0 and 4.0. An overlap of all raw force curves obtained in the absence and presence of $Cu^{2+}$ cations and at the physiological condition, pH 7.4, is shown in the left column of Fig. 2. Clustered data points at certain rupture lengths and rupture forces represent visual presentations of the overlay of multiple rupture events and provide a clear comparison between the presence and absence of $Cu^{2+}$ cations. Major differences between these two types of experiments are highlighted with colored light pink or light blue vertical bands.

In the absence of $Cu^{2+}$ cations, the most probable contour length was 53.6 ± 9.7 nm (Fig 2; middle column). This value includes the length of the flexible tethers used for the peptide immobilization and the length of the stretchable segment of the peptide between the N–terminus and the peptide segment involved in the dimer stabilization (Yu et al. 2011; Yu et al. 2008; Lyubchenko et al. 2010; Kim et al. 2011). According to Fig. 1a, the total length of the tethers is 26.5 ± 3.0 nm (Supplementary material); therefore we estimate the contour length of the stretchable segment of Aβ42 molecule at these conditions to be 13.6 ± 5.1 nm per Aβ42 molecule. Given the length of each amino acid as 0.34–0.4 nm, we estimate that more than a half of the N-terminus of the peptide is unstructured and undergoes stretching. In the presence of $Cu^{2+}$ cations, the most probable contour length decreased to 31.6 ± 3.5 nm, which corresponds to a stretchable segment length of 2.6 ± 2.3 nm, or 5–7 aa (amino acids) per Aβ42 molecule. This suggests that $Cu^{2+}$ cations alter the folding pattern of Aβ42

dimers resulting in the inclusion of the entire N-terminus. This structural change is accompanied by a 15% increase in rupture forces.

The central motivation of this work was to investigate the effect of $Cu^{2+}$ cations on the early stages of Aβ aggregation. Careful comparison of force results has been made between $Cu^{2+}$–present and $Cu^{2+}$–free experiments. In the absence of $Cu^{2+}$, the N terminus (D1 K16) as well as the central hydrophobic cluster (L17–A21) of Aβ42 peptides were found not to be involved in interpeptide interactions. By contrast, these two parts were brought to form Aβ dimer complexes by $Cu^{2+}$. This finding was in line with a recent study, in which the N terminus of Aβ was observed to participate the formation of β–sheet conformation (Haupt et al. 2012).

The shift in the contour length values induced by $Cu^{2+}$ cations also was observed at pH 5.0 (Fig. 3a), with a 40% increase in the rupture force. A similar pattern was observed at pH 6.8 (Supplementary Fig. S1) and pH 6.0 (Supplementary Fig. S2). Additionally, for pH values from 7.4 to 5.0, the statistical average yields of rupture events in the presence of $Cu^{2+}$ cations were at least two times higher than those in the $Cu^{2+}$–free experiments, suggesting that $Cu^{2+}$ cations promote the dimerization of Aβ42. Experiments performed at pH 4.0 (Fig. 3b) demonstrate that $Cu^{2+}$ cations have minimal effects on Aβ2 interactions under these conditions. Thus, $Cu^{2+}$ cations promote the dimerization of Aβ42 over the pH range of 7.4–5.0, but this effect is not observed at more acidic pH. This finding is consistent with the results obtained by other methods that demonstrated that $Cu^{2+}$ cations did not interact with Aβ when the pH was below 5.0 (Atwood et al. 1998).

### Effect of $Cu^{2+}$ cations on Aβ42 aggregation

We used AFM imaging to directly inspect the effect of $Cu^{2+}$ cations on Aβ aggregation at later stages. We incubated 10 μM Aβ solutions under quiescent conditions at all pH values studied above and imaged aliquots taken at various times during the aggregation process.

At pH 7.4, long fibrils with heights of 4.6 nm appeared on the $6^{th}$ day in the presence of substoichiometric $Cu^{2+}$ cations (Fig 4a, black arrows). Shorter and thinner fibrils were also observed (profibrils), as indicated with red arrows. These fibrillar features were found in the absence of $Cu^{2+}$ cations (Fig. 4b). Bright globular features (oligomers) were observed, as indicated with green arrows. A corresponding quantitative analysis of Aβ aggregates is shown in Fig. 4c. A large proportion of fibrils were observed by AFM in the presence of $Cu^{2+}$ cations, suggesting that $Cu^{2+}$ cations promote Aβ aggregation in the elongation phase. At pH 5.0, Aβ fibrils appeared in experiments with and without $Cu^{2+}$ cations (Fig. 5a and 5b). However, the percentage of fibrils in the presence of $Cu^{2+}$ cations was significantly larger (21%) than that in the control experiment (4%), as shown in Fig 5f and 5e. Fibrils were observed both in the absence and presence of $Cu^{2+}$ cations after 5 days of incubation at pH 4.0 (Fig 5c and 5d). These results are consistent with our force spectroscopy data that demonstrated no effects of $Cu^{2+}$ under these conditions. The fibril populations in both experiments were similar (Fig 5g and 5h), even though images were acquired at arbitrarily chosen spots that may have different surface coverage. In the present study, a long lag phase for fibril growth was found at pH 4.0 and 7.4; consistent with the notion that pH 5.0 is the optimum condition for A aggregation in contrast to pH 4.1 and pH 7.0–7.4 (Snyder et al. 1994).

## Discussion

### $Cu^{2+}$ cations change the structure of Aβ42 dimers

AFM force spectroscopy revealed that $Cu^{2+}$ cations dramatically change the folding pattern of Aβ42 within dimers. In the absence of the cations, the monomers are stabilized by the

interactions of peptide segments located at the C-terminus of the peptide. Assuming the dimers are symmetrically formed, the linker length analysis shows that in the absence of $Cu^{2+}$ cations the N-terminal segment of the peptide up to Ser26 is not involved with interpeptide interactions. The addition of $Cu^{2+}$ cations dramatically decreases the non-interacting regions, shortening the N-terminal region to Arg5–Asp7. The pattern is essentially similar in the pH range between pH 7.4 and pH 5.0. Additionally, in the presence of $Cu^{2+}$ cations, dimer stability is increased, dependent on pH. At pH 7.4, the increment on rupture force is approximately 15%; however, at pH 5.0, the value increases by a factor of three. The finding that the peptide N–terminus is involved in dimer stabilization is consistent with early studies that have shown that three histidine residues at the N–terminus are the major $Cu^{2+}$ coordination sites (Shin and Saxena 2008). Copper, in its oxidized form, $Cu^{2+}$, causes the pKa value of the imidazole of the histidine residue to decrease from 14 to approximately 7. This change enables protonation of the imidazole and the coordination of $Cu^{2+}$ cations over a broad pH range (Rauk 2009; Ali-Torres et al. 2011). In addition to the three histidine residues, Asp1 (Hong et al. 2010), Ala2 (Drew et al. 2009), Glu3 (Miura et al. 2004), Asp7 (Sarell et al. 2009), Tyr10 (Stellato et al. 2006), Glu11 (Streltsov et al. 2008), and Val40 (Parthasarathy et al. 2011) were also reported to be the coordination site. Therefore, a plausible explanation of the rupture observed with short contour lengths is that the coordination of $Cu^{2+}$ to N–terminal residues leads to a conformational change of Aβ42 that significantly facilitates the intrapeptide contact.

On the basis of these findings, we propose a model of $Cu^{2+}$ cation mediated structural transitions of Aβ42 into misfolded states, as shown schematically in Fig. 6. In the absence of $Cu^{2+}$ cations, the dimer is stabilized by the interactions of the Aβ42 C–termini, schematically shown by two arrows (Fig. 6a). With a strong rupture force these two segments can form antiparallel β-sheet structures. Shortening of the non-structured N-termini suggests that in the presence of $Cu^{2+}$ cations, monomeric Aβ42 folds and these folded conformers interact with each other, as shown schematically in Fig. 6b. We assume that this conformation is close to the one found for Aβ42 structures in fibrils. The Glu11-Lys16 N-terminal region of this structurally different monomeric unit is involved in an intramolecular antiparallel β–sheet structure (Ahmed et al. 2010). This is in agreement with the contour length analysis that indicates the rupture position at Arg5–Asp7. Additionally, a β–turn exists at the Asp23–Lys28 region (Lazo et al. 2005; Ahmed et al. 2010). This model is consistent with a prevailing pathway for $Cu^{2+}$ induced Aβ aggregation, in which $Cu^{2+}$ cations induce a conformational change from mostly random coils through a partially helical conformation to a partially β–sheet structure (Yang et al. 2006). The circular dichroism experiments have demonstrated that intermediates with partial α–helix and β–sheet structures exist during the transition from monomers to fibrils before rapid aggregation (Kirkitadze et al. 2001; Fezoui and Teplow 2002). This conformational change is also supported by the solution studies of the Aβ peptide structure by Fourier transform infrared spectroscopy (Stroud et al. 2012), solution NMR spectroscopy (Olofsson et al. 2009), and mass spectroscopy (Murariu et al. 2007).

Other than the conformational change pathway, other possible pathways of $Cu^{2+}$ cation induced Aβ aggregation include: 1) catalysis of dimer formation (via dityrosines) by radical chemistry (Murakami et al. 2005; Smith et al. 2007); 2) bridging of a histidine residue by two metal ions (Smith et al. 2006); and 3) change of overall net charge (Sarell et al. 2010; Syme et al. 2004). In our experiments, radical chemistry is not possible because we did not use reductants. Second, the likelihood of the bridging effect is low as the rupture forces in the presence of $Cu^{2+}$ cations were less than 50 pN. With the level of force loading rates used in our force measurements, breaking an interpeptide metal coordination bond often generates moderate rupture forces (58 pN) (Beyer and Clausen-Schaumann 2005; Schmitt et al. 2000). $Cu^{2+}$ cations may alter the net charge of Aβ42 because this peptide possesses a net

charge of −3 under physiological conditions (Rauk 2009). $Cu^{2+}$–induced charge neutralization could result in a strong propensity for peptide self-association. This could explain our force spectroscopy results at 7.4; however, this would not be consistent with our results obtained at mildly acidic pH in which the Aβ42 pI was 5.4, and the fact that stronger aggregation effects were observed at pH 5.0 than at pH 7.4. Another model suggests that $Cu^{2+}$ cations change the positive charge density at the N-terminus of Aβ42. Enhanced charge density may conversely raise the proportion of β–structure (Klug et al. 2003; Rauk 2009). This notion is more practically consistent with the conformational change model than other models.

### Substoichiometric concentrations of $Cu^{2+}$ cations accelerate Aβ42 aggregation

In addition to the effect of $Cu^{2+}$ cations on Aβ misfolding, $Cu^{2+}$ changes the pattern of later stages of peptide aggregation by facilitating fibril formation at pH 7.4 that does not appear in the absence of $Cu^{2+}$ cations. AFM imaging reveals fibrils in the absence of $Cu^{2+}$ cations at pH 5.0 because aggregation is facilitated by acidic condition. However, in the presence of $Cu^{2+}$ cations, the yield of fibrils is significantly higher than that in metal–free systems, suggesting that $Cu^{2+}$ cations are still capable of promoting Aβ42 aggregation under these conditions (Fig. 5e and 5f). At pH 4.0, samples in the presence and absence of $Cu^{2+}$ cations both show similar aggregation behavior, indicating that the aggregation effects of $Cu^{2+}$ are lost. These findings, along with the force spectroscopy results, suggest that $Cu^{2+}$ cations facilitate all stages of Aβ aggregation. The appearance of fibrils in the presence of $Cu^{2+}$ cations may require both dilute concentrations (not higher than 10 μM) and substoichiometric amounts of $Cu^{2+}$ cations (Masters and Selkoe 2012). Amorphous aggregates are commonly reported in previous studies due to the use of relatively high Aβ concentrations (usually 50–100 μM) (Miura et al. 2000; Tougu et al. 2011). A recent study has demonstrated that 2 μM Aβ in the presence of substoichiometric $Cu^{2+}$ cations was still sufficient for fibril growth. The authors proposed that the low peptide concentration required for fibril formation in the presence of $Cu^{2+}$ cations is reminiscent of the crystallization of proteins (Sarell et al. 2010), in which high protein concentrations lead to a high propensity for overt precipitation rather than ordered crystals. Similarly, suprastoichiometric amounts of $Cu^{2+}$ cations could cause excessive cross-linking of Aβ42, resulting in formation of amorphous aggregates or higher–order oligomers (Jones and Mezzenga 2012).

In conclusion, our AFM force spectroscopy and imaging results suggest that $Cu^{2+}$ cations increase interpeptide interactions; therefore it is reasonable to assume that $Cu^{2+}$ cations promote both the initial and the elongation phases of Aβ42 aggregation. Importantly, the single molecule force spectroscopy studies directly demonstrate the alterations in peptide conformation in the misfolded dimers and how the N–terminal residues aid in dimer stabilization. These findings may have relevance for understanding disease mechanisms and potential therapeutic strategies, such as metal dyshomeostasis (Bush and Tanzi 2008; Kenche and Barnham 2011).

## Supplementary Material

Refer to Web version on PubMed Central for supplementary material.

## Acknowledgments

We thank A. Krasnoslobodtsev, A. Portillo, Zenghan Tong, Yuliang Zhang and other group members for insightful suggestions and discussions. The work was supported by grants to Y.L.L. from the National Institutes of Health (NIH: GM096039), U.S. Department of Energy Grant DE-FG02-08ER64579, the Nebraska Research Initiative and grants to D.B.T. from NIH (NS038328, AG041295) and the Jim Easton Consortium for Drug Development and Biomarkers.

## References


Ahmed M, Davis J, Aucoin D, Sato T, Ahuja S, Aimoto S, Elliott JI, Van Nostrand WE, Smith SO. Structural conversion of neurotoxic amyloid-beta(1–42) oligomers to fibrils. Nat Struct Mol Biol. 2010; 17(5):561–567.10.1038/nsmb.1799 [PubMed: 20383142]

Ali-Torres J, Rodriguez-Santiago L, Sodupe M. Computational calculations of pKa values of imidazole in Cu(II) complexes of biological relevance. Phys Chem Chem Phys. 2011; 13(17):7852–7861.10.1039/c0cp02319a [PubMed: 21445432]

Atwood CS, Moir RD, Huang X, Scarpa RC, Bacarra NM, Romano DM, Hartshorn MA, Tanzi RE, Bush AI. Dramatic aggregation of Alzheimer abeta by Cu(II) is induced by conditions representing physiological acidosis. J Biol Chem. 1998; 273(21):12817–12826.10.1074/jbc.273.21.12817 [PubMed: 9582309]

Barnham KJ, Masters CL, Bush AI. Neurodegenerative diseases and oxidative stress. Nat Rev Drug Discov. 2004; 3(3):205–214.10.1038/nrd1330 [PubMed: 15031734]

Beyer MK, Clausen-Schaumann H. Mechanochemistry: the mechanical activation of covalent bonds. Chem Rev. 2005; 105(8):2921–2948.10.1021/cr030697h [PubMed: 16092823]

Bitan G, Kirkitadze MD, Lomakin A, Vollers SS, Benedek GB, Teplow DB. Amyloid beta -protein (Abeta) assembly: Abeta 40 and Abeta 42 oligomerize through distinct pathways. Proc Natl Acad Sci USA. 2003; 100(1):330–335.10.1073/pnas.222681699 [PubMed: 12506200]

Bush AI, Tanzi RE. Therapeutics for Alzheimer's disease based on the metal hypothesis. Neurotherapeutics. 2008; 5(3):421–432.10.1016/j.nurt.2008.05.001 [PubMed: 18625454]

Chen WT, Liao YH, Yu HM, Cheng IH, Chen YR. Distinct effects of Zn2+, Cu2+, Fe3+, and Al3+ on amyloid-beta stability, oligomerization, and aggregation: amyloid-beta destabilization promotes annular protofibril formation. J Biol Chem. 2011; 286(11):9646–9656.10.1074/jbc.M110.177246 [PubMed: 21216965]

Dobson CM. Protein folding and misfolding. Nature. 2003; 426(6968):884–890.10.1038/nature02261 [PubMed: 14685248]

Dong J, Canfield JM, Mehta AK, Shokes JE, Tian B, Childers WS, Simmons JA, Mao Z, Scott RA, Warncke K, Lynn DG. Engineering metal ion coordination to regulate amyloid fibril assembly and toxicity. Proc Natl Acad Sci USA. 2007; 104(33):13313–13318.10.1073/pnas.0702669104 [PubMed: 17686982]

Drew SC, Masters CL, Barnham KJ. Alanine-2 carbonyl is an oxygen ligand in Cu2+ coordination of Alzheimer's disease amyloid-beta peptide--relevance to N-terminally truncated forms. J Am Chem Soc. 2009; 131(25):8760–8761.10.1021/ja903669a [PubMed: 19496610]

Faller EM, Brown DL. Modulation of microtubule dynamics by the microtubule-associated protein 1a. J Neurosci Res. 2009; 87(5):1080–1089.10.1002/jnr.21920 [PubMed: 18951470]

Faller P. Copper and zinc binding to amyloid-beta: coordination, dynamics, aggregation, reactivity and metal-ion transfer. Chembiochem. 2009; 10(18):2837–2845.10.1002/cbic.200900321 [PubMed: 19877000]

Fezoui Y, Teplow DB. Kinetic studies of amyloid beta-protein fibril assembly. Differential effects of alpha-helix stabilization. J Biol Chem. 2002; 277(40):36948–36954.10.1074/jbc.M204168200 [PubMed: 12149256]

Gomez-Casado A, Dam HH, Yilmaz MD, Florea D, Jonkheijm P, Huskens J. Probing multivalent interactions in a synthetic host-guest complex by dynamic force spectroscopy. J Am Chem Soc. 2011; 133(28):10849–10857.10.1021/ja2016125 [PubMed: 21615157]

Haupt C, Leppert J, Ronicke R, Meinhardt J, Yadav JK, Ramachandran R, Ohlenschlager O, Reymann KG, Gorlach M, Fandrich M. Structural basis of beta-amyloid-dependent synaptic dysfunctions. Angew Chem Int Ed Engl. 2012; 51(7):1576–1579.10.1002/anie.201105638 [PubMed: 22234970]

Hong L, Carducci TM, Bush WD, Dudzik CG, Millhauser GL, Simon JD. Quantification of the binding properties of Cu2+ to the amyloid beta peptide: coordination spheres for human and rat peptides and implication on Cu2+-induced aggregation. J Phys Chem B. 2010; 114(34):11261–11271.10.1021/jp103272v [PubMed: 20690669]

Hong L, Simon JD. Insights into the thermodynamics of copper association with amyloid-beta, alpha-synuclein and prion proteins. Metallomics. 2011; 3(3):262–266.10.1039/c0mt00052c [PubMed: 21116546]

Huang X, Atwood CS, Moir RD, Hartshorn MA, Tanzi RE, Bush AI. Trace metal contamination initiates the apparent auto-aggregation, amyloidosis, and oligomerization of Alzheimer's Abeta peptides. J Biol Inorg Chem. 2004; 9(8):954–960.10.1007/s00775-004-0602-8 [PubMed: 15578276]

Hung YH, Bush AI, Cherny RA. Copper in the brain and Alzheimer's disease. J Biol Inorg Chem. 2010; 15(1):61–76.10.1007/s00775-009-0600-y [PubMed: 19862561]

Innocenti M, Salvietti E, Guidotti M, Casini A, Bellandi S, Foresti ML, Gabbiani C, Pozzi A, Zatta P, Messori L. Trace copper(II) or zinc(II) ions drastically modify the aggregation behavior of amyloid-beta1–42: an AFM study. J Alzheimers Dis. 2010; 19(4):1323–1329.10.3233/JAD-2010-1338 [PubMed: 20061619]

Jomova K, Vondrakova D, Lawson M, Valko M. Metals, oxidative stress and neurodegenerative disorders. Mol Cell Biochem. 2010; 345(1–2):91–104.10.1007/s11010-010-0563-x [PubMed: 20730621]

Jones OG, Mezzenga R. Inhibiting, promoting, and preserving stability of functional protein fibrils. Soft Matter. 2012; 8(4):876–895.10.1039/C1SM06643A

Kenche VB, Barnham KJ. Alzheimer's disease & metals: therapeutic opportunities. Br J Pharmacol. 2011; 163(2):211–219.10.1111/j.1476-5381.2011.01221.x [PubMed: 21232050]

Kim BH, Palermo NY, Lovas S, Zaikova T, Keana JF, Lyubchenko YL. Single-molecule atomic force microscopy force spectroscopy study of Abeta-40 interactions. Biochemistry. 2011; 50(23):5154–5162.10.1021/bi200147a [PubMed: 21553928]

Kirkitadze MD, Condron MM, Teplow DB. Identification and characterization of key kinetic intermediates in amyloid beta-protein fibrillogenesis. J Mol Biol. 2001; 312(5):1103–1119.10.1006/jmbi.2001.4970 [PubMed: 11580253]

Klug GM, Losic D, Subasinghe SS, Aguilar MI, Martin LL, Small DH. Beta-amyloid protein oligomers induced by metal ions and acid pH are distinct from those generated by slow spontaneous ageing at neutral pH. Eur J Biochem. 2003; 270(21):4282–4293.10.1046/j.1432-1033.2003.03815.x [PubMed: 14622293]

Krasnoslobodtsev AV, Shlyakhtenko LS, Lyubchenko YL. Probing Interactions within the synaptic DNA-SfiI complex by AFM force spectroscopy. J Mol Biol. 2007; 365(5):1407–1416.10.1016/j.jmb.2006.10.041 [PubMed: 17125791]

Lazo ND, Grant MA, Condron MC, Rigby AC, Teplow DB. On the nucleation of amyloid beta-protein monomer folding. Protein Sci. 2005; 14(6):1581–1596.10.1110/ps.041292205 [PubMed: 15930005]

Lin CJ, Huang HC, Jiang ZF. Cu(II) interaction with amyloid-beta peptide: a review of neuroactive mechanisms in AD brains. Brain Res Bull. 2010; 82(5–6):235–242.10.1016/j.brainresbull.2010.06.003 [PubMed: 20598459]

Lyubchenko YL, Kim BH, Krasnoslobodtsev AV, Yu J. Nanoimaging for protein misfolding diseases. Wiley Interdiscip Rev Nanomed Nanobiotechnol. 2010; 2(5):526–543.10.1002/wnan.102 [PubMed: 20665728]

Masters CL, Selkoe DJ. Biochemistry of Amyloid β-Protein and Amyloid Deposits in Alzheimer Disease. Cold Spring Harbor Perspectives in Medicine. 201210.1101/cshperspect.a006262

Miura T, Mitani S, Takanashi C, Mochizuki N. Copper selectively triggers beta-sheet assembly of an N-terminally truncated amyloid beta-peptide beginning with Glu3. J Inorg Biochem. 2004; 98(1):10–14.10.1016/j.jinorgbio.2003.10.008 [PubMed: 14659627]

Miura T, Suzuki K, Kohata N, Takeuchi H. Metal binding modes of Alzheimer's amyloid beta-peptide in insoluble aggregates and soluble complexes. Biochemistry. 2000; 39(23):7024–7031.10.1021/bi0002479 [PubMed: 10841784]

Murakami K, Irie K, Ohigashi H, Hara H, Nagao M, Shimizu T, Shirasawa T. Formation and stabilization model of the 42-mer Abeta radical: implications for the long-lasting oxidative stress in Alzheimer's disease. J Am Chem Soc. 2005; 127(43):15168–15174.10.1021/ja054041c [PubMed: 16248658]

Murariu M, Dragan ES, Drochioiu G. Synthesis and mass spectrometric characterization of a metal-affinity decapeptide: copper-induced conformational changes. Biomacromolecules. 2007; 8(12): 3836–3841.10.1021/bm700793g [PubMed: 17979241]

Olofsson A, Lindhagen-Persson M, Vestling M, Sauer-Eriksson AE, Öhman A. Quenched hydrogen/deuterium exchange NMR characterization of amyloid-β peptide aggregates formed in the presence of Cu2+ or Zn2+ FEBS Journal. 2009; 276(15):4051–4060.10.1111/j.1742-4658.2009.07113.x [PubMed: 19549187]

Olubiyi OO, Strodel B. Structures of the amyloid beta-peptides Abeta1-40 and Abeta1–42 as influenced by pH and a D-peptide. J Phys Chem B. 2012; 116(10):3280–3291.10.1021/jp2076337 [PubMed: 22300010]

Ono K, Condron MM, Teplow DB. Structure-neurotoxicity relationships of amyloid beta-protein oligomers. Proc Natl Acad Sci USA. 2009; 106(35):14745–14750.10.1073/pnas.0905127106 [PubMed: 19706468]

Parthasarathy S, Long F, Miller Y, Xiao Y, McElheny D, Thurber K, Ma B, Nussinov R, Ishii Y. Molecular-level examination of Cu2+ binding structure for amyloid fibrils of 40-residue Alzheimer's beta by solid-state NMR spectroscopy. J Am Chem Soc. 2011; 133(10):3390–3400.10.1021/ja1072178 [PubMed: 21341665]

Portillo AM, Krasnoslobodtsev AV, Lyubchenko YL. Effect of electrostatics on aggregation of prion protein Sup35 peptide. J Phys Condens Matter. 2012; 24(16): 164205.10.1088/0953-8984/24/16/164205 [PubMed: 22466073]

Rauk A. The chemistry of Alzheimer's disease. Chem Soc Rev. 2009; 38(9):2698–2715.10.1039/b807980n [PubMed: 19690748]

Rivera-Mancia S, Perez-Neri I, Rios C, Tristan-Lopez L, Rivera-Espinosa L, Montes S. The transition metals copper and iron in neurodegenerative diseases. Chem Biol Interact. 2010; 186(2):184–199.10.1016/j.cbi.2010.04.010 [PubMed: 20399203]

Roberts BR, Ryan TM, Bush AI, Masters CL, Duce JA. The role of metallobiology and amyloid-beta peptides in Alzheimer's disease. J Neurochem. 2012; 120(Suppl 1):149–166.10.1111/j.1471-4159.2011.07500.x [PubMed: 22121980]

Sarell CJ, Syme CD, Rigby SE, Viles JH. Copper(II) binding to amyloid-beta fibrils of Alzheimer's disease reveals a picomolar affinity: stoichiometry and coordination geometry are independent of Abeta oligomeric form. Biochemistry. 2009; 48(20):4388–4402.10.1021/bi900254n [PubMed: 19338344]

Sarell CJ, Wilkinson SR, Viles JH. Substoichiometric levels of Cu2+ ions accelerate the kinetics of fiber formation and promote cell toxicity of amyloid-{beta} from Alzheimer disease. J Biol Chem. 2010; 285(53):41533–41540.10.1074/jbc.M110.171355 [PubMed: 20974842]

Schmitt L, Ludwig M, Gaub HE, Tampe R. A metal-chelating microscopy tip as a new toolbox for single-molecule experiments by atomic force microscopy. Biophys J. 2000; 78(6):3275–3285.10.1016/S0006-3495(00)76863-9 [PubMed: 10828003]

Shin BK, Saxena S. Direct evidence that all three histidine residues coordinate to Cu(II) in amyloid-beta1-16. Biochemistry. 2008; 47(35):9117–9123.10.1021/bi801014x [PubMed: 18690709]

Smith DP, Ciccotosto GD, Tew DJ, Fodero-Tavoletti MT, Johanssen T, Masters CL, Barnham KJ, Cappai R. Concentration dependent Cu2+ induced aggregation and dityrosine formation of the Alzheimer's disease amyloid-beta peptide. Biochemistry. 2007; 46(10):2881–2891.10.1021/bi0620961 [PubMed: 17297919]

Smith DP, Smith DG, Curtain CC, Boas JF, Pilbrow JR, Ciccotosto GD, Lau TL, Tew DJ, Perez K, Wade JD, Bush AI, Drew SC, Separovic F, Masters CL, Cappai R, Barnham KJ. Copper-mediated amyloid-beta toxicity is associated with an intermolecular histidine bridge. J Biol Chem. 2006; 281(22):15145–15154.10.1074/jbc.M600417200 [PubMed: 16595673]

Snyder SW, Ladror US, Wade WS, Wang GT, Barrett LW, Matayoshi ED, Huffaker HJ, Krafft GA, Holzman TF. Amyloid-beta aggregation: selective inhibition of aggregation in mixtures of amyloid with different chain lengths. Biophys J. 1994; 67(3):1216–1228.10.1016/S0006-3495(94)80591-0 [PubMed: 7811936]

Sparks DL, Schreurs BG. Trace amounts of copper in water induce beta-amyloid plaques and learning deficits in a rabbit model of Alzheimer's disease. Proc Natl Acad Sci U S A. 2003; 100(19): 11065–11069.10.1073/pnas.1832769100 [PubMed: 12920183]

Stellato F, Menestrina G, Serra MD, Potrich C, Tomazzolli R, Meyer-Klaucke W, Morante S. Metal binding in amyloid beta-peptides shows intra- and inter-peptide coordination modes. Eur Biophys J. 2006; 35(4):340–351.10.1007/s00249-005-0041-7 [PubMed: 16404590]

Streltsov VA, Titmuss SJ, Epa VC, Barnham KJ, Masters CL, Varghese JN. The structure of the amyloid-beta peptide high-affinity copper II binding site in Alzheimer disease. Biophys J. 2008; 95(7):3447–3456.10.1529/biophysj.108.134429 [PubMed: 18599641]

Stroud JC, Liu C, Teng PK, Eisenberg D. Toxic fibrillar oligomers of amyloid-beta have cross-beta structure. Proc Natl Acad Sci USA. 201210.1073/pnas.1203193109

Sulchek TA, Friddle RW, Langry K, Lau EY, Albrecht H, Ratto TV, DeNardo SJ, Colvin ME, Noy A. Dynamic force spectroscopy of parallel individual Mucin1-antibody bonds. Proc Natl Acad Sci U S A. 2005; 102(46):16638–16643.10.1073/pnas.0505208102 [PubMed: 16269547]

Syme CD, Nadal RC, Rigby SE, Viles JH. Copper binding to the amyloid-beta (Abeta) peptide associated with Alzheimer's disease: folding, coordination geometry, pH dependence, stoichiometry, and affinity of Abeta-(1–28): insights from a range of complementary spectroscopic techniques. J Biol Chem. 2004; 279(18):18169–18177.10.1074/jbc.M313572200 [PubMed: 14978032]

Tougu V, Tiiman A, Palumaa P. Interactions of Zn(II) and Cu(II) ions with Alzheimer's amyloid-beta peptide. Metal ion binding, contribution to fibrillization and toxicity. Metallomics. 2011; 3(3): 250–261.10.1039/c0mt00073f [PubMed: 21359283]

Walsh DM, Lomakin A, Benedek GB, Condron MM, Teplow DB. Amyloid beta-protein fibrillogenesis. Detection of a protofibrillar intermediate. J Biol Chem. 1997; 272(35):22364–22372.10.1074/jbc.272.35.22364 [PubMed: 9268388]

Yang H, Pritzker M, Fung SY, Sheng Y, Wang W, Chen P. Anion effect on the nanostructure of a metal ion binding self-assembling peptide. Langmuir. 2006; 22(20):8553–8562.10.1021/la061238p [PubMed: 16981775]

Yu J, Lyubchenko YL. Early stages for Parkinson's development: alpha-synuclein misfolding and aggregation. J Neuroimmune Pharmacol. 2009; 4(1):10–16.10.1007/s11481-008-9115-5 [PubMed: 18633713]

Yu J, Malkova S, Lyubchenko YL. alpha-Synuclein misfolding: single molecule AFM force spectroscopy study. J Mol Biol. 2008; 384(4):992–1001.10.1016/j.jmb.2008.10.006 [PubMed: 18948117]

Yu J, Warnke J, Lyubchenko YL. Nanoprobing of alpha-synuclein misfolding and aggregation with atomic force microscopy. Nanomedicine. 2011; 7(2):146–152.10.1016/j.nano.2010.08.001 [PubMed: 20817126]

Zou J, Kajita K, Sugimoto N. Cu(2+) Inhibits the Aggregation of Amyloid beta-Peptide(1–42) in vitro. Angew Chem Int Ed Engl. 2001; 40(12):2274–2277.10.1002/1521-3773(20010618)40:12<2274::AID-ANIE2274>3.0.CO;2–5 [PubMed: 11433492]

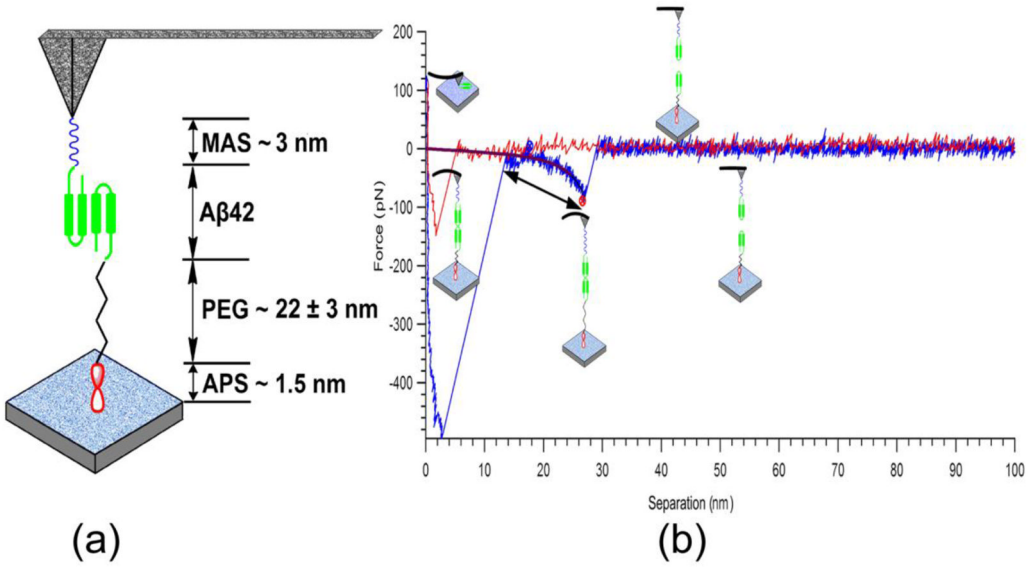


**Figure 1.**

Experimental setup of SMFS (a). One of the interacting Aβ42 molecules is immobilized on the APS modified mica surface via a long PEG linker. The counterpart Aβ42 molecule is anchored on the MAS functionalized AFM tip. A typical approach–retraction cycle of recorded rupture force curve (b). The rupture events and the polymer stretching segment of the force curve are indicated with a single-headed arrow and a double headed arrow, respectively.

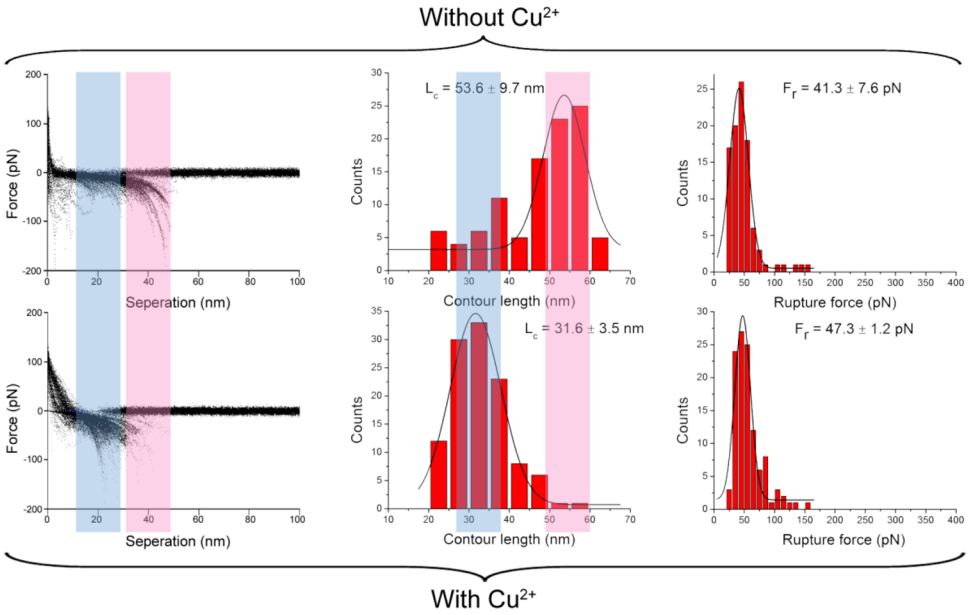


**Figure 2.**

AFM force spectroscopy in the presence and absence of $Cu^{2+}$ cations at pH 7.4. The force spectroscopy in the absence of $Cu^{2+}$ cations is shown in the upper panel. The columns include, from left to right: the overlap of all raw force curves, the distribution of contour length, and the distribution of rupture force. The lower panel shows the corresponding characteristic of force spectroscopy in the presence of $Cu^{2+}$ cations. The $L_c$ and $F_r$ denote the most probable contour length and the most probable rupture force, respectively.

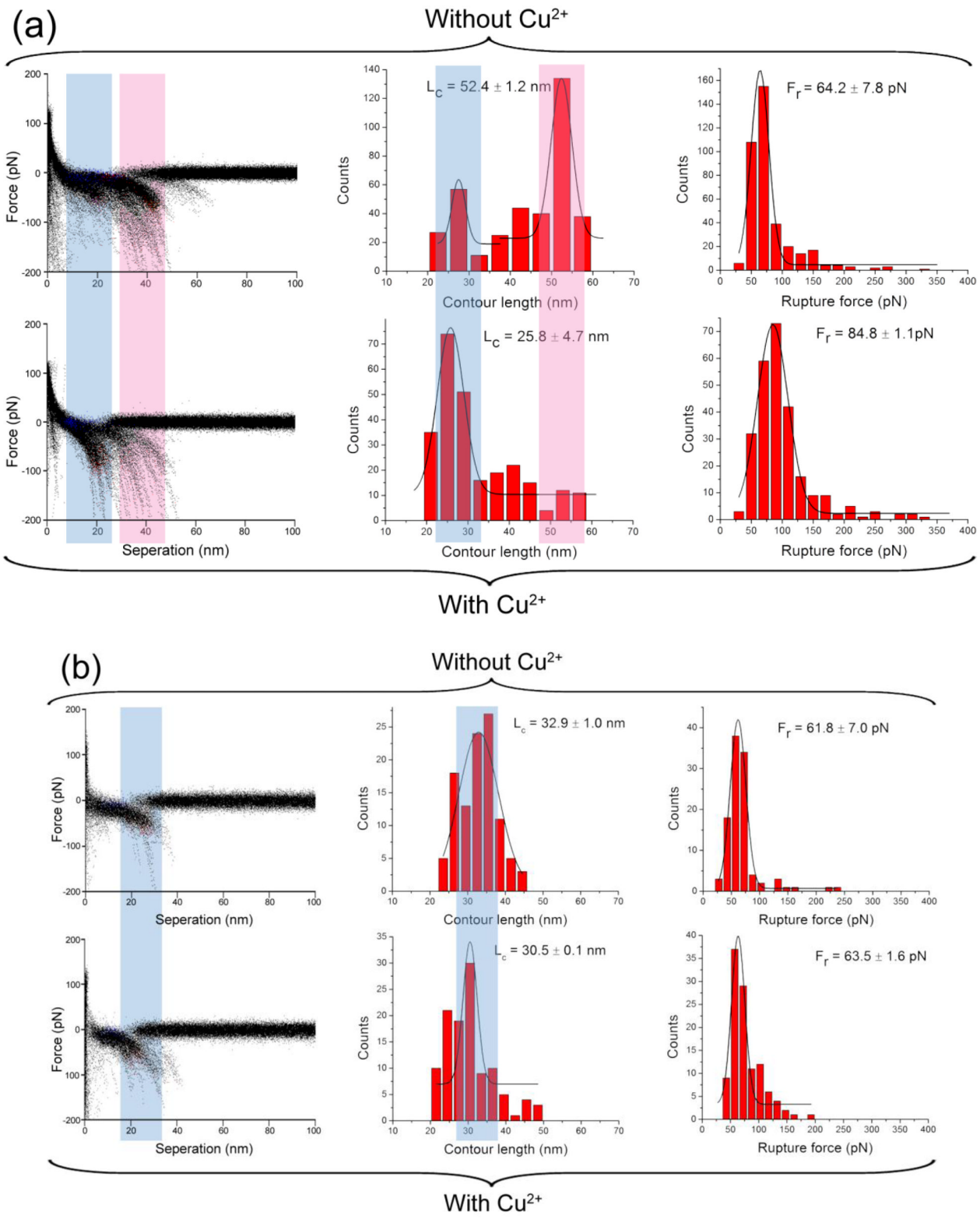


**Figure 3.**

AFM force spectroscopy in the presence and absence of $Cu^{2+}$ cations at pH 5.0 is shown in (a). The force spectroscopy in the absence of $Cu^{2+}$ cations is shown in the upper panel. The columns include, from left to right: the overlap of all raw force curves, the distribution of contour length, and the distribution of rupture force. The lower panel shows the corresponding characteristic of force spectroscopy in the presence of $Cu^{2+}$ cations. Similar SMFS results in the presence and absence of $Cu^{2+}$ cations at pH 4.0 are shown in (b). The $L_c$ and $F_r$ denote the most probable contour length and the most probable rupture force, respectively.

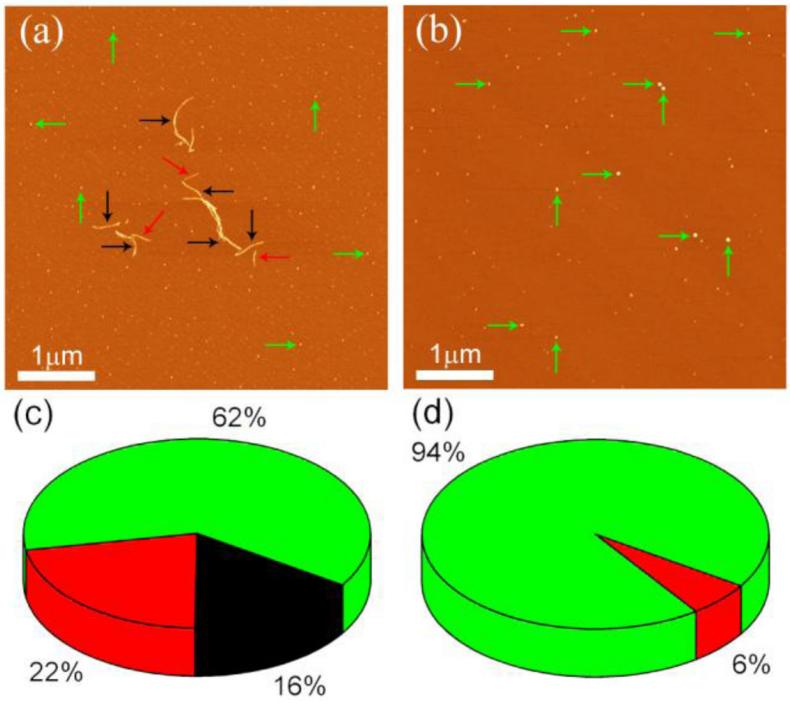


**Figure 4.**

Representative AFM images of Aβ42 aggregates in the presence (a) and absence (b) of $Cu^{2+}$ cations at pH 7.4. Yields of aggregates formed in the presence of $Cu^{2+}$ cations (c) and absence of $Cu^{2+}$ cations (d) are shown in pie charts. Mature fibrils, protofibrils and oligomers are colored in black, red, and green, respectively.

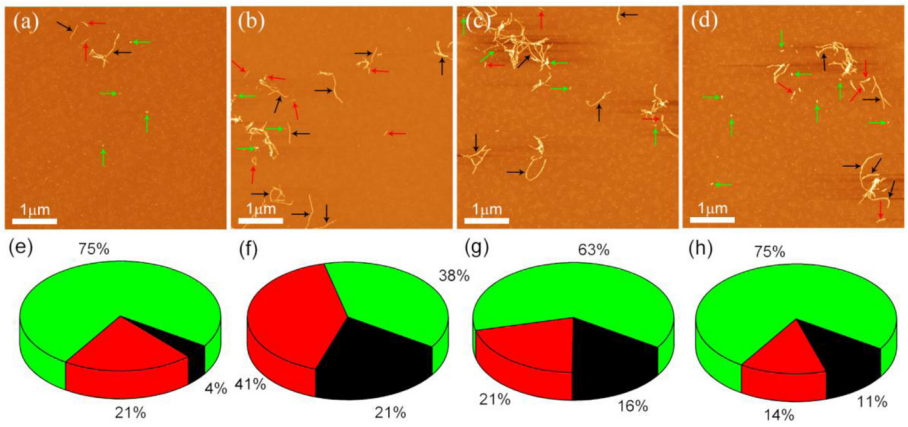


**Figure 5.**

(a) and (b) show representative AFM images of Aβ42 aggregates in the absence and presence of $Cu^{2+}$ cations at pH 5.0, respectively. Representative AFM images of Aβ42 aggregates in the absence (c) and presence (d) of $Cu^{2+}$ cations at pH 4.0. Yields of aggregates formed in the absence of $Cu^{2+}$ cations (e) and presence of $Cu^{2+}$ cations (f) are shown in pie charts. Mature fibrils, protofibrils and oligomers are colored in black, red, and green, respectively. (g) and (h) show the yields of aggregates formed in the absence of $Cu^{2+}$ cations and presence of $Cu^{2+}$ cations, respectively.

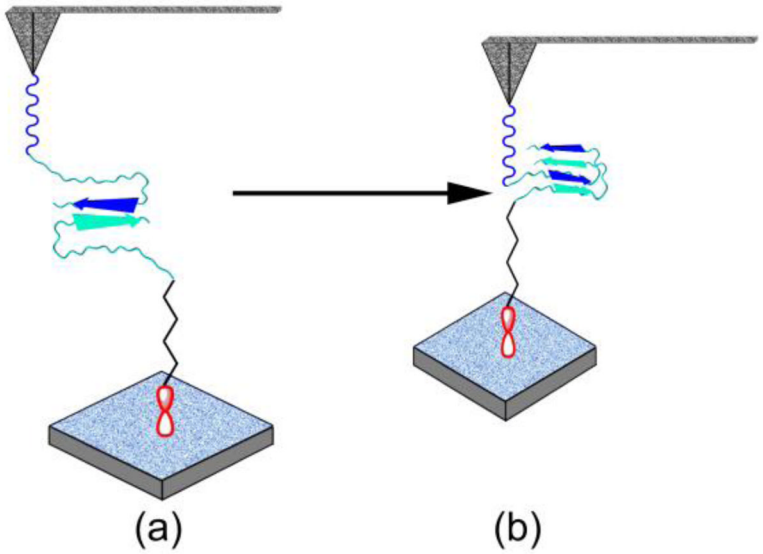


**Figure 6.**

Schematic view of the proposed structure model of Aβ42 dimer formation in the absence (a) and presence (b) of $Cu^{2+}$ cations. The structure of $Cu^{2+}$–free dimers is characterized by an interpeptide interaction between the two hydrophobic C–termini of the Aβ42 peptides. With $Cu^{2+}$, the dimers adopt a compact structure highlighted by an interpeptide parallel β-sheet structure.

**Table 1**

Summary of the most probable contour length (MPCL) and the most probable rupture force (MPRF) of force spectroscopy in the presence and absence of $Cu^{2+}$ cations at all pH.

| | MPRF (pN) | | MPCL (nm) | |
|---|---|---|---|---|
| | **without Cu** | **with Cu** | **without Cu** | **with Cu** |
| pH 7.4 | 41.3 ± 7.6 | 47.3 ± 1.2 | 53.6 ± 9.7 | 31.6 ± 3.5 |
| pH 6.8 | 41.6 ± 2.0 | 50.2 ± 2.6 | 50.7 ± 3.9 | 32.0 ± 9.2 |
| pH 6.0 | 53.3 ± 2.1 | 77.2 ± 2.5 | 45.4 ± 1.8 | 28.1 ± 5.5 |
| pH 5.0 | 64.2 ± 7.8 | 84.8 ± 1.1 | 52.4 ± 1.2 | 25.8 ± 4.7 |
| pH 4.0 | 61.8 ± 7.0 | 63.5 ± 1.6 | 32.9 ± 1.0 | 30.5 ± 0.1 |